REAL-TIME SMALL-SIZE SPACE DEBRIS DETECTION WITH EISCAT RADAR FACILITIES

J Markkanen and M Postila

Executive Summary
of
ESOC Contract No. 16646/02/D/HK(CS)
with
EISCAT Scientific Association

ESA/ESOC Technical Management
M Landgraf

February 2005

Generated from LaTeX source, February 24, 2005.

Contents

1 Overview

1.1 Introduction

It is estimated that there are approximately 200,000 objects larger than 1 cm currently orbiting the Earth, as an enduring heritage of four decades of space activity. This includes the functioning satellites, but by far most of the objects are what is called space debris (SD), man-made orbital objects which no longer serve any useful purpose. Many of the small-sized (less than 10 cm) particles are due to explosions of spacecraft and rocket upper stages, but there are also exhaust particles from solid rocket motors, leaked cooling agents, and particles put into space intentionally for research purposes. The large (> 10 cm) objects have known orbits and are routinely monitored by the US Space Surveillance Network, but information of the smaller particles is fragmentary and mainly statistical. Especially, in Europe there is no radar that is routinely used for monitoring small-size SD.

In 2000-2001, we, together with our colleagues from Sodankylä Geophysical Observatory, undertook a study for ESA about the feasibility of using the EISCAT ionospheric research radars for space debris measurements [3]. Since the early 1980's, the EISCAT mainland radars—the Tromsø UHF radar at latitude 69.6°N, operating at 930 MHz and the VHF radar operating at 225 MHz—have been performing ionospheric measurements to the order of 2000 hours per year; and since the late 1990's, after the EISCAT Svalbard radar (latitude 78.2°N) became operational, EISCAT has been measuring more than 3000 hours annually. The interest is to use a substantial amount of these operating hours for simultaneous space debris measurements in a cost-effective way. In the initial study, we showed that it is feasible, and technically straightforward, to perform

SD measurements in parallel with normal EISCAT ionospheric measurements, without interfering with those measurements [8].

Our measuring approach is to operate a separate digital receiver back-end, which we call the SD receiver, in parallel with EISCAT standard digital receiver. This allows us to implement our own, amplitude domain data processing, which we call the the match function or matched-filtering (MF) method. The MF method makes use of the long coherence time of a signal reflected from a small target to increase detection sensitivity, via pulse-to-pulse coherent integration. To make the hardware as simple and cheap as possible, the custom-made part of the SD receiver is basically just a fast sampler and digital demodulator; the MF computations are done in fast but still cheap general purpose workstations. The SD receiver samples the EISCAT analog signal, at the second intermediate frequency (10 MHz) level, fast enough to capture the relevant frequency channels into a single digital stream, without doing the customary channel separation. Typically during a measurement, we sample at the rate of about a million complex samples per second continuously, producing more than 10 GBytes of data per hour. Early on, ESA suggested that we should strive to do the data analysis in real-time so that the raw data could be quickly disregarded.

A straightforward implementation of the MF method involves Fourier-transforming long data vectors, a few thousand times per every second of raw data; basically, one is computing power spectra for a relatively large number of range gates. At the Space Debris III conference in 2001, we had to concede that with the processing speed that we had achieved at the time, it would take several centuries of CPU time to analyze just one year's quota of EISCAT space debris measurements. However, soon afterwards, M Lehtinen of Sodankylä Geophysical Observatory, who was the project leader of the precursor study, realized that by accepting some loss of detection sensitivity and a small bias in the velocity estimate, it would be possible to speed up the MF computation drastically, typically by more than two orders of magnitude. We use the term fast match function algorithm (FMF) for the resulting computing scheme.

The results of the initial study were encouraging. The achieved detection sensitivity was equivalent to being able to observe spherical targets with diameters of about 2 cm from 1000 km range. With the advent of the FMF-algorithm, the processing speed, though still sluggish, was starting to become useful. In 2003, ESA commenced the present study, to bring the analysis of large amounts of EISCAT SD data up to real-time speed [4]. The study has achieved the necessary processing speed. In addition to the factor of 100 delivered by the FMF algorithm, we now use computers that are about ten times faster than what we had available in 2001. A final required factor of ten was obtained by coding the MF and FMF algorithms in C instead of Matlab.

The EISCAT system [1, 2, 10] consists of three separate radars: monostatic VHF radar, located near Tromsø, Norway, and operating at 224 MHz; monostatic but two-antenna EISCAT Svalbard Radar in Longyerbyen, Svalbard, operating at 500 MHz; and tristatic EISCAT UHF radar at 930 MHz, with transmitter in Tromsø and receivers in Tromsø and in Kiruna, Sweden, and Sodankylä, Finland. All the transmitters operate in the megawatt peak power range and routinely utilize high (10–20%) duty cycles.

Even though routinely picking-up hard target echoes, standard EISCAT data processing is not optimized for hard targets. The characteristic feature expected from small hard targets is a long signal coherence time, several hundred milliseconds. By a signal's (phase-) coherence we mean that the signal phase $\phi_0(t)$ obeys a deterministic functional form for some length of time, the coherence time.

EISCAT's normal ionospheric signal has coherence time of less than a millisecond in most parts of the ionosphere. This time is much shorter than the interval between transmitted pulses, the interpulse period (IPP), which in EISCAT typically is 5–10 ms. Therefore, echoes from individual pulses are uncorrelated, and can only be added up in the power domain. This is done by computing, for each of the received pulses separately, signal autocorrelation functions, or, equivalently, power spectra, for a set of range gates, and then adding these power-domain quantities. This is called non-coherent pulse-to-pulse integration. We note that within a *single* transmission-reception (T/R) cycle, computing range-gated power spectra achieves coherent integration of the samples. For a single non-coded pulse, the MF method, too, in effect just computes range-gated power spectra.

To achieve coherent integration from pulse to pulse, the MF method adds the echoes from different T/R cycles in amplitude domain and takes care that the pulses are added with equal phase. The method, in essence, removes *all* phase variation from the signal before adding the samples. This is achieved by guessing the phase factor $e^{i\phi_0(t)}$ of the signal, and canceling it by multiplying the signal by the complex conjugate of the guess, $e^{-i\phi_0(t)}$. The guesses in our implementation are generated by brute force. We search through a large set of parametrized model functions, and use the one which achieves best cancellation of the phase, that is, which results in the largest integrated amplitude. After the phase variation has successfully been removed, the remaining part of the signal can be safely integrated, both within a single pulse, as well as from pulse to pulse.

As long as the signal stays coherent (obeys the assumed model), coherent integration suppresses the non-coherent background noise, so that the effective signal-power to noise-power ratio increases directly proportionally to the number of pulses integrated. This increases detection sensitivity. Non-coherent integration, instead, does not increase the signal-to-noise ratio (but it, too, increases the detection sensitivity, by reducing the likelihood of false alarms). The drawback in coherent integration, in addition of it being computationally more demanding due to the long data vectors, is that if the signal model is not accurate, the ensuing phase error will start eating into the integrated signal amplitude, rendering longer integration useless.[1] In our case, coherent integration beyond about 300 ms does not seem to improve detection sensitivity.

Part of the reason for the unexpectedly short apparent coherence time is that, although we (see section 2.3) will derive a signal model that should be fairly accurate for small structureless targets, for performance reasons we cannot actually use the ideal model. The approximative model that we do use, both in the MF and FMF algorithms, is best suited for narrow-band (single-frequency-channel) transmissions. The different frequency channels in a multi-frequency signal will have slightly different Doppler-shifts because the Doppler-shift depends on the transmission frequency. It is impossible to cancel the Doppler phase factors simultaneously using only the single model phase factor which is available in the approximative model.

We derive in section 2.1 the MF method via Bayesian statistical inversion. Within the Bayesian approach, the estimates for the basic parameters range, radial velocity, radical acceleration, and signal amplitude or signal total energy, are found as the most probable values, given the measured noisy signal. With our assumptions, this solution is also the one that minimizes the least squares norm between the measured signal and the set of

[1] We admit that there may be a grain of truth in the statement in a recent book which claims that "most radars utilize non-coherent integration", because "maintaining coherency [...] is very costly and challenging to achieve." [7]

model functions; the solution is also the maximum likelihood solution.

We have, in four measurement campaigns during the two years of this study, collected and analysed about 150 hours of data, all at the EISCAT UHF radar in Tromsø. These data have been taken mostly for method development and verification purposes; assessing any possible physical significance of the about 2500 events that we have accumulated is outside the scope of this work. By way of example only, we will show some of the analysis results in chapter 4. We show that the peak detection rate is about 2.5 events per hour per 50 km bin near 1000 km altitude (Fig. 8 on p. 26). We show that we observe events down to effective diameter of about 21–22 mm at 1000 km range (Fig. 9 on p. 27). We must emphasize, however, that all our results concerning target sizes are, at best, lower bounds; we cannot say anything about the actual target cross sections. For perhaps the single major deficiency in EISCAT, compared with some other radars used for space debris observations, is that the EISCAT antennas do not have monopulse feed. At the moment at least, there is no way that would allow pinpointing the actual direction of the target within the radar beam, and so the target's radar cross section cannot be deduced from the measured signal strength. We hope that in the future we can partly alleviate this problem by collecting fairly large amounts of data—perhaps about 10,000 events per year—so that the antenna beam pattern can be taken into account statistically, and meaningful comparisons to space debris models made. Finally, we also plot target velocity and acceleration as function of altitude (Fig. 10–11).

1.2 Study objectives

According to our contract agreement with ESA/ESOC [4], the objective of this study was

"To develop methods to perform real-time detection of small-sized debris objects in LEO during routine EISCAT operations. The new methods shall be based on the capabilities (soft- and hardware, as well as data processing procedures) for debris detection that have been developed in the precursor study. The routine real-time detection shall be demonstrated during standard EISCAT experiment campaigns."

1.3 Summary

After a feasibility study in 2000–2001 about using EISCAT radars to detect centimetre-sized space debris in the frame of an ESA contract, the present study was aimed at boosting the debris detection and parameter estimation to real-time speed. A requirement in the work is to piggy-back space debris measurements on top of EISCAT's normal ionospheric work, without interfering with those measurements, and to be able to handle on the order of 500 hours of measurements per year.

We use a special digital receiver back-end in parallel with EISCAT's standard digital receiver. We sample fast enough to correctly band-pass sample the EISCAT analog frequency band at the second IF level. To increase detection sensitivity, we use amplitude domain integration—coherent pulse-to-pulse integration—of the samples. The coherent integration is built into our method of target parameter estimation, which we call the MF method, for match function or matched filtering. The method is derived from Bayesian statistical inversion. With common assumptions about the noise and the prior, the method reduces to minimizing with respect to the parameters amplitude b, range R, radial velocity v and radial acceleration a the norm $\|z(t) - b\chi(R, v, a; t)\|$, where z is the measured signal and $b\chi(t)$ is a model signal. Because the model signal depends linearly

on b, it is sufficient to maximize the magnitude of the inner product between z and χ, the amplitude estimate is then determined by direct computation. The magnitude of the inner product, when properly normalized, is the MF.

Our original Matlab implementation of the MF method in the precursor study was about four orders of magnitude too slow for real-time applications. In this study, we have gained the required speed factors. A factor of ten comes from using faster computers, another factor of ten comes from coding our key algorithms in plain C instead of Matlab. The largest factor, typically 100–300, comes from using a special, approximative, but in practice quite sufficient, method of finding the MF maximum. Test measurements show that we get real-time speed already when using a single 2 GHz dual-processor G5 Macintosh to do the detection computations.

The measurement campaigns also show that the achieved sensitivity at the EISCAT UHF radar, which has a radar wavelength of 32 cm, corresponds to detecting a 2.2 cm diameter target at the range of 1000 km. We register typically 15–25 targets per hour in the 500–1500 km altitude band. A final 101 h debris measurement campaign, conducted in parallel with a standard EISCAT ionospheric experiment in November 2004, confirmed that we can now handle longish measurements essentially in real-time.

There remain partially open issues, like the efficiency of the coherent integration in the theory sector; the need for more robust and automated execution of the experiments in the software sector; and the need to ensure the availability of eventual replacement of our special receiver in the hardware sector. Nevertheless, we are now technically in the position to start routine space debris measurements with the EISCAT system.

2 Theory

2.1 The match function method

We want to estimate the parameters of a hard target echo signal $s(t)$ in the presence of white gaussian noise $\gamma(t)$, of variance σ^2, in an optimal way. We denote by $z(t)$ the received signal,

$$z(t) = s(t) + \gamma(t)\,. \tag{1}$$

We denote by $x(t)$ the transmission sample signal (the signal labeled by TS in Fig. 5 on p. 19). We ignore the frequency translations done in the actual space debris receiver and treat all these quantities as complex-valued (demodulated) signals.

To find an optimal estimate, we will use the approach of Bayesian statistical inversion. The basic idea is to use a parametrized model for s and find the most probable signal among the model signals, given the measured signal z. We specify the model signals explicitly in section 2.3. Here we will make use only of the property that the model depends linearly on one parameter, the complex amplitude b, and in addition depends on some other parameters (range R, radial velocity v and radial acceleration a in our case), which we collectively denote by θ, so that

$$s(t) = b \cdot \chi(\theta; t). \tag{2}$$

We sample $z(t)$ using sampling interval τ_s and get N samples z_n during a time interval T_c, the integration time.

After a measurement has produced a result, the vector z, some signal parameter values (b, θ) will be considered more likely than others, in a way that depends on z. The probability of the parameter values is described by a conditional probability density, with z as the condition. In the Bayesian world view, that density is termed the posteriori density, and we denote it here by $D_{\mathrm{p}}(b, \theta|z)$. The inversion problem is to utilize the measurement result to find the posteriori density. The posteriori density is the most complete inference that can be made about the parameter values, based on the measurement. Normally, one wants to condense the inference to single numbers, the parameter estimates, together with some simple measures of errors like some confidence intervals. There is no unique way to select "best" estimates, but the standard Bayesian criterion is to use the most probable values, that is, the maximum of the posteriori density:

$$(\widehat{b}, \widehat{\theta}) = \arg\max_{b,\theta} D_{\mathrm{p}}(b, \theta|z). \tag{3}$$

We now derive the posteriori density. We denote by $D_1(z_n|s_n)$ the conditional probability density of z_n, given s_n. This is just the probability distribution of the value of the nth noise sample $\gamma_n = z_n - s_n$,

$$D_1(z_n|s_n) = \frac{1}{\pi\sigma^2} \mathrm{e}^{-\frac{1}{\sigma^2}|z_n - s_n|^2}. \tag{4}$$

We assumed that the noise is white so that the noise samples are uncorrelated. Then the conditional joint probability density to produce a particular measurement result vector z if the actual signal vector is s, is

$$D(z|s) = \prod_{n=0}^{N-1} D_1(z_n|s_n) = \frac{1}{(\pi\sigma^2)^N} \cdot \mathrm{e}^{-\frac{1}{\sigma^2}\|z-s\|^2}. \tag{5}$$

The density $D(z|s)$ is called the direct theory. Given the direct theory, the Baysian solution to the inversion problem is

$$D_{\mathrm{p}}(b, \theta|z) = C'(z) \cdot D_{\mathrm{pr}}(b, \theta) \cdot D(z|s). \tag{6}$$

Here $C'(z)$ is a normalization factor. The new factor, $D_{\mathrm{pr}}(b, \theta)$, is called the prior density. The prior density is a weight that can be used if it is known a priori—before making the measurement—that some particular signals $s(b, \theta)$ tend to occur more frequently than some others.[2] Using a non-trivial D_{pr} might actually make sense when measuring space debris, to throw out detections with highly unlikely parameters. But so far we have assumed a constant prior. For a constant prior, it follows from Eq. (6) and Eq. (5) that the sought-for posteriori density is

$$D_{\mathrm{p}}(b, \theta|z) = C(z) \cdot \mathrm{e}^{-\frac{1}{\sigma^2}\|z - b\cdot\chi(\theta)\|^2}, \tag{7}$$

where $C(z)$ is a normalization factor. It follows from Eq. (7) that finding the most probable signal parameters amounts to minimizing the distance between the measurement and the models,

$$(\widehat{b}, \widehat{\theta}) = \arg\min_{b,\theta} \|z - b \cdot \chi(\theta)\|. \tag{8}$$

[2] $D_{\mathrm{pr}}(b, \theta)$ is, by definition, equal to the marginal density $\int D_{\mathrm{tot}}(b, \theta, z)\, dz$ of the probability distribution $D_{\mathrm{tot}}(b, \theta, z)$, the probability distribution of the whole system, which contains on equal footing both the measurement results z and the signals $s(b, \theta)$.

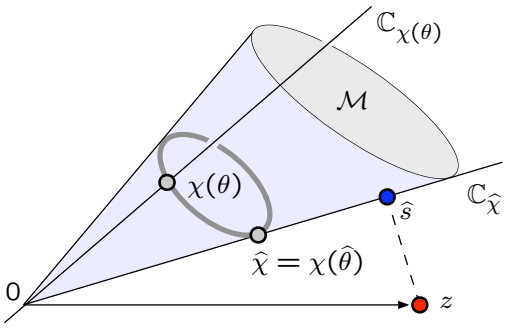

Figure 1: Geometric interpretation of the MF method. The sought-for best estimate of the signal is the point $\widehat{s}$ in the set $\mathcal{M}$ of model functions that is nearest to the measured signal z. The set $\mathcal{M}$ consists of rays $\mathbb{C}_\chi = \{a\chi \colon a \in \mathbb{C}\}$, generated by a set of basic model signals $\chi(\theta)$. The $\mathrm{MF}(\theta)$ is defined as the length of the orthogonal projection of z onto the ray $\mathbb{C}_{\chi(\theta)}$. Maximizing $\mathrm{MF}(\theta)$ gives the ray $\mathbb{C}_{\widehat{\chi}}$ that gets as near to the point z as is possible in $\mathcal{M}$. The estimate $\widehat{s}$ is the orthogonal projection of z onto $\mathbb{C}_{\widehat{\chi}}$.

A straightforward approach to the minimization problem expressed in Eq. (8) is to discretize the parameter space and perform an exhaustive search. We now show that the search space dimension can be reduced by one by making use of the property that the amplitude b enters the problem linearly. Our result can be confirmed analytically, but will be here reasoned from basic vector geometry. Referring to Fig. 1, the set $\mathcal{M}$ of model vectors $\{b\,\chi(\theta)\}$ consists of 1-dimensional rays $\mathbb{C}_\chi$ through the origin of N-dimensional complex vector space $\mathbb{C}^N$. The rays are generated by a set of basic vectors $\chi(\theta)$. According to Eq. (8), we need to find the shortest distance between the measured point z and $\mathcal{M}$. The figure suggests that we first find the ray $\mathbb{C}_{\widehat{\chi}}$ that is as parallel as possible with the vector z; then the point in $\mathcal{M}$ that is nearest to z is the orthogonal projection $\widehat{s}$ of z onto $\mathbb{C}_{\widehat{\chi}}$,

$$\widehat{s} = \frac{\langle z, \widehat{\chi}\rangle}{\|\widehat{\chi}\|^2}\widehat{\chi}\,. \tag{9}$$

So the real problem is to find the maximally parallel ray. With z fixed, a sufficient measure of parallelism of a ray $\mathbb{C}_\chi$ and the vector z is the length of the orthogonal projection of z onto χ; the ray is the more parallel or antiparallel, the longer the projection. This particular measure of parallelism is what we call the match function MF,[3]

$$\mathrm{MF}(\theta) = \frac{|\langle z, \chi(\theta)\rangle|}{\|\chi(\theta)\|}\,. \tag{10}$$

We get the maximally parallel model vector $\widehat{\chi} = \chi(\widehat{\theta})$ by maximizing the function $\mathrm{MF}(\theta)$:

$$\widehat{\theta} = \arg\max_\theta \mathrm{MF}(\theta)\,. \tag{11}$$

[3]Intuitively, the more parallel two signal vectors (functions) are, the more they presumably look alike, which is one reason for our nomenclature. A more serious reason is that MF stands for matched filter. With velocity and acceleration fixed, so that MF is function of the range variable only, $R \mapsto \langle z, \chi(R)\rangle$ amounts to ordinary filtering of z by the filter $h(t) = \chi(0)(t)$ that is matched to the transmitted signal. The MF is a generalization of this concept to more general kind of pattern matching.

How the maximum is computed in practice is discussed in section 2.4; basically, we perform an exhaustive search over a grid of values of θ.

2.2 Energy-to-noise ratio and detection threshold

The energy W_y of any correctly sampled complex-valued voltage signal $y(t)$ is

$$W_y = \int |y(t)|^2 dt = \tau_\mathrm{s} \sum |y_n|^2 = \tau_\mathrm{s} \|y\|^2 \,. \tag{12}$$

From Eq. (9)–(11), the energy $W_{\widehat{s}}$ of the signal estimate $\widehat{s}$ is

$$\frac{W_{\widehat{s}}}{\tau_\mathrm{s}} = \|\widehat{s}\|^2 = \frac{|\langle z, \widehat{\chi}\rangle|^2}{\|\widehat{\chi}\|^2} = [\mathrm{MF}(\widehat{\theta})]^2 = \max \mathrm{MF}^2. \tag{13}$$

In all our data analysis we have used $W_{\widehat{s}}$ as the estimator of the signal energy W_s. We summarize the match function method of parameter estimation

- Get the signal parameters θ by locating the position of MF maximum, Eq. (11).
- Get the signal energy as the square of the value of the MF maximum, Eq. (13).

A noise-free MF is useful for theoretical considerations. Without noise, both factors in the inner product in Eq. (10) are model functions. We reserve a separate notation, AF, and use the standard name, ambiguity function [9], for the noise-free match function,

$$\mathrm{AF}(\theta_0; \theta) = \frac{|\langle \chi(\theta_0), \chi(\theta)\rangle|}{\|\chi(\theta)\|} \,. \tag{14}$$

In the MF method, target detection is based on the estimated signal energy $W_{\widehat{s}}$ exceeding a threshold. We have so far set the threshold, by visual inspection of the data, to be so high that there are only very few false alarms. We need to use a range-dependent threshold, because the lower altitudes, typically up to about 500 km, are often affected by strong clutter from the ionosphere, and need a higher threshold.

We set the detection threshold in terms of a dimensionless quantity, the ratio of signal energy to the noise power spectral density (PSD) G_γ. We call this ratio the energy-to-noise ratio, and denote it by $\mathrm{SNR_N}$,

$$\mathrm{SNR_N} = \frac{W_s}{G_\gamma} \,. \tag{15}$$

We assume that the system noise temperature T_sys is defined in such a way that the noise PSD density of complex-valued wide-band noise can be written as

$$G_\gamma = kT_\mathrm{sys} \,, \tag{16}$$

where k is the Boltzmann constant. The power of such a noise after being filtered with a boxcar-shaped low-pass filter that extends from frequency $-B/2$ to $B/2$ is

$$P_\gamma = kT_\mathrm{sys}B. \tag{17}$$

The digitally implemented filter in the SD receiver is boxcar-shaped in time, not in frequency. Its impulse response has constant value $1/\tau_\mathrm{s}$ and duration τ_s. For such a

filter, it can be shown that the noise-equivalent bandwidth B_{eq} is equal to the sampling frequency, so that, on the one hand we have

$$B_{\mathrm{eq}} = \frac{1}{\tau_{\mathrm{s}}}\,, \tag{18}$$

and on the other hand, B_{eq} also satisfies Eq. (17), by definition of the noise equivalence. From Eq. (16)–(18) and (13) we get

$$\frac{W_{\widehat{s}}}{kT_{\mathrm{sys}}} = \frac{W_{\widehat{s}} \cdot B_{\mathrm{eq}}}{kT_{\mathrm{sys}} \cdot B_{\mathrm{eq}}} = \frac{(\max \mathrm{MF}^2 \cdot \tau_{\mathrm{s}}) \cdot (1/\tau_{\mathrm{s}})}{P_\gamma} = \frac{\max \mathrm{MF}^2}{P_\gamma}. \tag{19}$$

We treat the system temperature as a known radar parameter, and use Eq. (19) with the measured $\max \mathrm{MF}$ and P_γ to find the signal energy W_s in physical units. We use that estimate to find a lower limit, $\mathrm{RCS}_{\mathrm{min}}$, for the target's radar cross section (RCS). From the standard radar equation it follows

$$\mathrm{RCS} = \frac{(4\pi)^3\, kT_{\mathrm{sys}} \cdot R^4 \cdot \mathrm{W_s}}{G(\phi)^2 \cdot \lambda^2 \cdot P_x \cdot \mathcal{D}T_c}\,. \tag{20}$$

Here R is target range, λ is radar wavelength, P_x transmission power, $\mathcal{D}$ transmission duty cycle so that $\mathcal{D}T_c$ is the actual length of transmission during the integration T_c. The factor $G(\phi)$ is the antenna power gain in the direction of the target within the radar beam, an angle ϕ offset from the known direction of the antenna optical axes. In the EISCAT system, it is normally not possible to find the offset angle. As a way of cataloguing the observed signal strength, we therefore normally quote $\mathrm{RCS}_{\mathrm{min}}$, which we get from Eq. (20) by setting $\phi = 0$.

The energy estimate $W_{\widehat{s}}$ defined in Eq. (13) is a biased estimate. In typical situations, the expectation value $\mathrm{E}W_{\widehat{s}}/\tau_{\mathrm{s}}$ is larger than W_s/τ_{s} by as much as about ten times the mean background noise power P_γ. The positive bias in the energy estimate means that the $\mathrm{RCS}_{\mathrm{min}}$ is not quite as bad a substitute for the RCS as it would otherwise in most cases be.

2.3 Signal model

We model the phase of the received SD echo $s(t)$ by assuming that the phase behaves as if the signal would reflect from a mirror that moves with constant radial acceleration a_0. We will assume that during an integration time T_{c} the signal amplitude b stays constant. With $x(t)$ the transmission sample signal and t' the delayed time, with reference to Fig. 2 we take

$$s(t) = bx(t')\,. \tag{21}$$

For any given target radial motion $r(t)$, the delayed time is determined by

$$t - t' = \frac{2r(\frac{t'+t}{2})}{c}\,. \tag{22}$$

With constant radial acceleration, the target range is

$$r = r(R_0, v_0, a_0; t) = R_0 + v_0 t + \frac{1}{2} a_0 t^2\,. \tag{23}$$

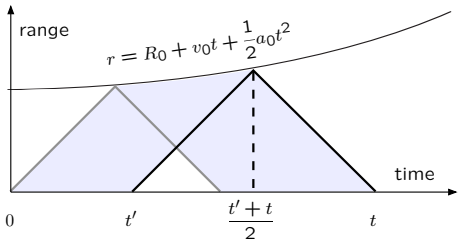

Figure 2: Transmitted wave reflected from a point-like target which is moving with constant radial acceleration a_0. The parabola shows the radial component of the target's position vector in the coordinate frame of a stationary radar antenna, during the few hundred milliseconds of a coherent integration. The full three-dimensional velocity vector typically is very nearly constant in that frame during the integration time. The integration starts at time 0 with the transmission of the first pulse belonging to the integration. At the start of the integration, target range is R_0 and radial velocity is v_0. The diagram is not drawn to scale.

For the motion (23), Eq. (22) is quadratic in t'. The solution of the equation for the pulse propagation time $t - t'$, with an appropriate choice of the sign of the square root, is

$$t - t' = \frac{2c}{a_0} \left\{ 1 + \frac{v_0}{c} + \frac{a_0}{c} t - \left[1 + \frac{2v_0}{c} + \left(\frac{v_0}{c} \right)^2 + \frac{2a_0}{c} (t - \frac{R_0}{c}) \right]^{\frac{1}{2}} \right\} . \tag{24}$$

Equation (24) can be simplified by expanding the square root $[\ldots]^{\frac{1}{2}}$ into a power series. Care must be exercised regarding to which terms can be dropped from the expansion. With parameter values that are typical at EISCAT UHF when antenna is pointed nearly vertically,

$$\begin{aligned} R_0 &\approx 10^6 \text{ m}, \\ v_0 &\approx 10^3 \text{ m s}^{-1}, \\ a_0 &\approx 10^2 \text{ m s}^{-2}, \\ \omega_1 &\approx 6 \cdot 10^9 \text{ Hz}, \end{aligned}$$

all terms following the "1" inside the square brackets in Eq. (24) are quite small compared to unity. But what actually determines which terms X can be ignored, is the requirement that the corresponding phase factor $\omega_1 \frac{2c}{a_0} X$, where ω_1 is the radar transmission frequency, stays very small during the integration time. Using the first three terms of the power series expansion of $[1 + (\ldots)]^{\frac{1}{2}}$, and then dropping all the individual terms for which the corresponding phase factor is less than 0.1 rad when integration time is less than a second, we are left with

$$t - t' \approx \frac{2}{c} \left[R_0 + v_0 t + \frac{1}{2} a_0 t^2 - (v_0 + a_0 t) \frac{R_0}{c} \right] \tag{25}$$

$$= \frac{2}{c} \left[R_0 + v_0 (t - \frac{R_0}{c}) + \frac{1}{2} a_0 (t - \frac{R_0}{c})^2 \right] \tag{26}$$

$$= \frac{2}{c} r (t - \frac{R_0}{c}) . \tag{27}$$

The term $\frac{-R_0}{c}$ is a natural first order correction to the time instant of pulse reflection; the only non-trivial aspect is that this correction already is sufficient (for our typical measuring configurations). Thus, the model functions $\chi(R, v, a; t)$ to be used in the MF computation, Eq. (10), are of the form

$$\chi(R, v, a; t) = x(t - \frac{2}{c}\, r(R, v, a;\, t - \frac{R}{c}))\,. \tag{28}$$

It should be noted that *nothing* has been assumed about the transmission $x(t)$ in this derivation so far. In principle, as long as the transmission can be accurately measured via the transmission sample signal, we do not even need (ever) to know what transmission has been used; the MF machinery incorporates the transmission transparently. This is a good thing for automated piggy-back measurements, where we do not have any control on the transmission EISCAT might be using at any given time.

The reality, of course, is somewhat different. A basic problem is that the radar's noise-environment is often poorly approximated by our assumption that it consists only of stationary gaussian noise. Distortions occur in practice, one of them being the ionosphere becoming visible in the SD data. More or less ad hoc, manual, experiment-specific solutions are used to counter these problems. Also, we cannot at the moment handle the case that the antenna pointing may change during a measurement; but many EISCAT measurements use cyclical antenna pointing schemes. In practice, both now and into the foreseeable future, we need to know beforehand the EISCAT measurements that we are making use of in the SD work.

2.4 Computational aspects

Here we derive the approximation for the signal model, which we have been using in our work so far. Assume that the transmission can be described as

$$x(t) = \epsilon(t)\mathrm{e}^{i\omega_1 t}\,, \tag{29}$$

where ω_1 is the carrier frequency, and the transmission envelope $\epsilon(t)$ is a slowly changing function, describing, say, a binary phase modulation, as is often the case in EISCAT. This description is good for a single-frequency-channel transmission. We ignore the correction $-R/c$ to the pulse reflection time in Eq. (28), and use the special form Eq. (29) of the transmission to write the model function as

$$\chi(t) = \epsilon(t - \frac{2}{c} r(t))\, e^{i\omega_1 [t - \frac{2}{c} r(t)]}\,. \tag{30}$$

Inside the slowly varying transmission envelope we can assume $r(t)$ stays constant, $r(t) = R$, during the integration time. Then, from Eq. (30) and Eq. (29), it follows that

$$\chi(t) \;\; = \;\; x(t - \frac{2R}{c})\, \mathrm{e}^{i(\omega_\mathrm{D} t + \alpha_\mathrm{D} t^2)}\,, \tag{31}$$

where $\omega_\mathrm{D} = -\omega_1 \frac{2v}{c}$ and $\alpha_\mathrm{D} = -\omega_1 \frac{a}{c}$ are the Doppler-frequency, and the rate of change of the Doppler-frequency, which we will call the Doppler-drift, respectively. The approximation (31) is often used in the literature (usually without the drift term), and is described by saying that the received signal is a delayed-in-time, Doppler-shifted replica

of the transmission. With the signal model (31), the MF definition in Eq. (10) can be expanded for continuous-time signals as

$$\mathrm{MF}(R,v,a) = \frac{|\int_0^{T_\mathrm{c}} z(t)\overline{x}(t-\frac{2R}{c})\mathrm{e}^{-i(\omega_\mathrm{D}t+\alpha_\mathrm{D}t^2)}\,dt|}{\sqrt{W_\mathrm{x}}}\,, \tag{32}$$

where $W_\mathrm{x} = \int |x(t)|^2 dt$ is the energy of the transmission sample signal.

For signal vectors, we need to take into account that the transmission samples x_n are only available at times $n\tau_\mathrm{s}$. This already forces us to discretize the range variable. With

$$R_j = j \cdot \frac{c\tau_\mathrm{s}}{2} \tag{33}$$

the match function becomes

$$\mathrm{MF}(R_j,v,a) = \frac{|\sum_{n=0}^{N-1} z_n\overline{x}_{n-j}\mathrm{e}^{-i(\omega_\mathrm{d}n+\alpha_\mathrm{d}n^2)}|}{\|x\|}\,, \tag{34}$$

where the normalized Doppler-shift and Doppler-drift are

$$\omega_\mathrm{d} = -\omega_1\tau_\mathrm{s}\frac{2v}{c}\,, \tag{35}$$

$$\alpha_\mathrm{d} = -\omega_1\tau_\mathrm{s}\frac{a\tau_\mathrm{s}}{c}\,. \tag{36}$$

At the points

$$v_k = k\frac{2\pi c}{\omega_1 T_\mathrm{c}} \tag{37}$$

Eq. (34) can be written as

$$\mathrm{MF}(R_j,v_k,a) = \frac{|\sum_{n=0}^{N-1}(z_n\overline{x}_{n-j}\mathrm{e}^{-i\alpha_\mathrm{d}n^2})\mathrm{e}^{-i\frac{2\pi kn}{N}}|}{\|x\|}\,, \tag{38}$$

which shows that at these points the MF can be evaluated using FFT. The denominator $\|x\|$ is the square root of transmission sample energy, and is (of course) independent of R, v and a.

In most of our data analysis, we have taken the radial acceleration to be a deterministic function of range, $a = a(R)$. We have used the acceleration that corresponds to the target being on a circular orbit and the antenna being pointed vertically. Experimentation with real data has shown that not much sensitivity is lost in practice even if the acceleration is not varied.[4]

In the routine analysis therefore, we search the MF maximum only over the (R_j, v_k)-grid. Even then, the detection computations, using full resolution and without any further approximation, become too large. Assume we want to cover 1000 km in range and use 0.3 s coherent integration. Assume that the sampling interval is 0.5 μs. Then the

[4] Which is perhaps a bad sign, because a priori, we expect the MF maximum value to be rather sensitive to the acceleration being correct. For instance, inspection of the ambiguity functions indicate that with 0.3 s integration, a 10 $\mathrm{m\,s^{-2}}$ error in a would cause the coherently integrated amplitude to drop by about 50% from the ideal case. That this appears not to happen when we vary the acceleration in the analysis of real data, suggests that there are other factors that are causing the signal model to be incorrect to begin with. One of these factors is related to multi-frequency transmission, as discussed in section 2.6.

input data vector is 600,000 points, and the FFT requires about 60 million floating-point operations. The $1000/0.075 \approx 13,000$ range gates require about 800×10^9 floating-point operations. On a dual-processor 2 GHz G5 Mac, we get about 1 GFlops combined speed in FFT of this length, so we will need about 800 s to handle the 0.3 s of data. A normal EISCAT UHF phase-coded transmission uses baud length of about 20 μs or more. For these modulations, we can safely relax the range gate separation in the detection phase somewhat, say by a factor of 10 (this also ensures sufficient Doppler-frequency coverage). But this still leaves us more than two orders of magnitude short of real-time speed.

2.5 The fast match function algorithm

Since spring 2001 we have used the fast match function algorithm, FMF, for all our practical target detection computations. We showed in [8] that in practice we do not lose much accuracy even if we use the FMF also for parameter estimation, at least when the estimates can be done by fitting to multiple points of time series data. (Things might be different when we only have a single point available—as can happen for the weakest signals.) By using the FMF, which is about 300 times faster than the MF in a typical situation, we can easily achieve real-time speed for the overall data processing. When we want to use MF for parameter estimation, we do that offline.

The original purpose was to use the FMF for target detection purposes. Therefore, the FMF was designed to give a good approximation of the MF near its absolute maximum position. Especially, to preserve detection sensitivity, it is important that the FMF achieves coherent integration to a good approximation. If there is only a single frequency in the transmission, it can be shown that $\max \mathrm{FMF}$ is not smaller than about 60% of the fully coherently integrated amplitude. We will comment on the more realistic case of dual-frequency transmission in the next section; the result is that even in multifrequency situation, the FMF is not seriously worse than the MF, but then both algorithms will fall short from fully coherent integration.

We make use of two special properties of our measuring situation in EISCAT: the property that we are using a pulsed radar; and the property that the space debris receiver "oversamples" the debris signal heavily. The quotes are needed, for the high sampling rate is necessary to correctly sample the multi-frequency transmission. But we are oversampling with respect to the Doppler-shifted, inherently narrow-band signal on any given frequency channel. The time consuming part of the MF evaluation is to compute the velocity slices, that is, the power spectra for a set of range gates. We make use of the two properties to drastically reduce the length of the FFT input vectors.

First, we note that the Doppler-velocity interval that we need to monitor is much narrower than the interval that is actually available with the high sampling rates f_s that we use in the SD receiver. For the 930 MHz radar frequency (0.32 m wavelength), the benchmark 2 MHz sampling gives unambiguous velocities in the interval $\pm(f_s/2)\cdot(\lambda/2) = \pm 160\ \mathrm{km\,s^{-1}}$. Typically, for near-vertical pointing, it suffices to monitor velocity interval $\pm 5\ \mathrm{km\,s^{-1}}$. Therefore, for each range gate j, we can downsample (decimate) the to-be-Fourier-transformed vector w, which according to Eq. (38) is formed from transmission samples x_n, signal samples z_n, and an acceleration correction term $\exp(-i\alpha_j n^2)$,

$$w_n = z_n \overline{x}_{n-j} \mathrm{e}^{-i\alpha_j n^2}\,, \tag{39}$$

by a factor M_{dec}, which is $160/5 = 32$ for 2 MHz sampling, and 8 for the more typical 0.5 MHz sampling. We do the decimation by forming a new sequence w'_n by adding

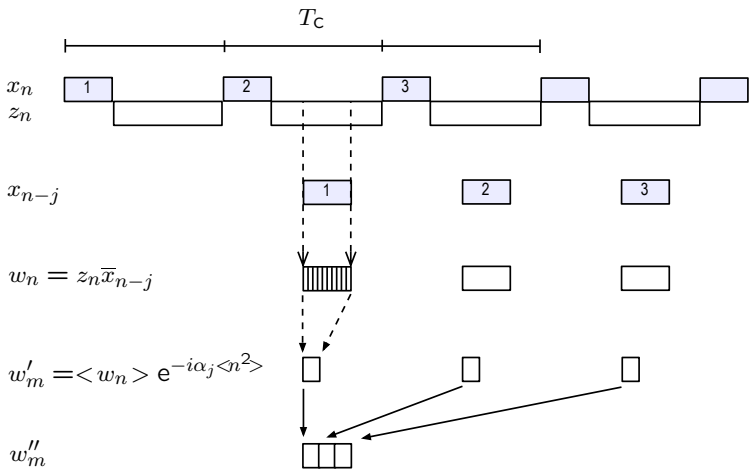

Figure 3: Forming the Fourier-transform input vector for a given range gate in the FMF algorithm. For each of M IPP's (M=3 in the figure), one first forms the point-wise product w of the reception z and the shifted, complex-conjugated transmission $\overline{x}$. Next, for each IPP, w is decimated, and the decimated vector multiplied by an appropriate mean acceleration correction factor to get the vector w'. Finally, the w'-vectors from the IPPs are concatenated to form the input vector w''.

w_n's in blocks of M_{dec}. At the same time, we make use of the fact that within such a block, the acceleration factor is almost constant. For each block we use the average phase ϕ' within the block and take $\exp(-i\phi')$ out of the decimation sum. This reduces both the number of multiplications and the number of complex exponentials that need to be evaluated.

Second, we make use of the fact that most of the elements of w are zeros, in known locations. When we form w' from w, we only compute and decimate the products (39) at the points where we know there can be non-zero data. The transmission duty cycle in EISCAT experiments is about 10% in the UHF and about 20% at ESR. Therefore, about 80–90% of the elements of w are zeros, in regularly placed blocks. We now simply concatenate the non-zero blocks of w'. We get a vector w'', which typically is two orders of magnitude shorter than the original FFT input vector w. For example, in the benchmark case with 600,000 point raw data input vector, using decimation factor 15 as we normally do, w'' has the length $N'' = (1/15) \cdot 0.1 \cdot 600,000 = 4000$. Finally, we Fourier-transform and normalize w'' to get the FMF at range gate R_j and Doppler-frequency ω,

$$\mathrm{FMF}(R_j, \omega) = \frac{|\sum_{n=0}^{N''-1} w''_n e^{-i\omega\tau_s n}|}{\|x\|} . \tag{40}$$

By restricting ω to the points $\omega_k = 2\pi k/(N''\tau_s)$, the FMF can be evaluated using FFT. This is the fast match function algorithm. Due to the much shorter FFT input vector, even allowing for the extra computations needed in decimation, the FMF is 100–300 times faster than the MF in typical cases. The computation of the FFT input vector w'' in Eq. (40) is summarized in Fig. 3.

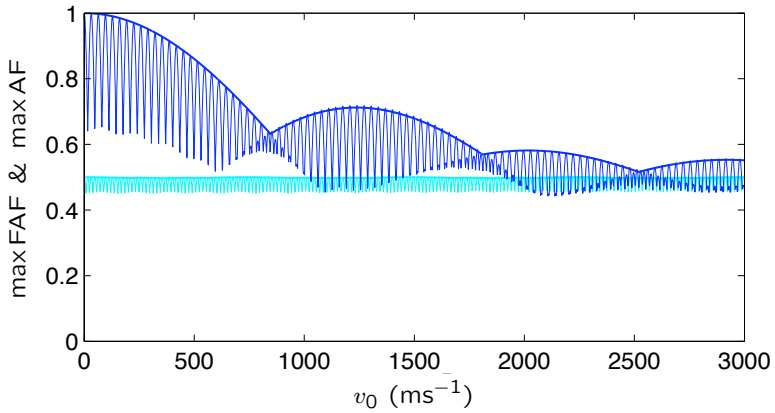

Figure 4: Failure of coherent integration in standard dual-frequency tau2 measurements. We plot the maximum value of the FAF (fast oscillating blue curve) and the AF (slowly oscillating envelope curve, with larger line width) as a function of the target's radial velocity. Normalization is such that unity represents fully coherent integration. The integration time is 300 ms. With increasing target velocity, both max AF and max FAF approach the single-channel level. The single-channel case is shown with the cyan curves at the near-constant value of about one-half; for that data, the value 0.5 represents fully coherent integration. The single-channel curves were computed by setting one of the two frequency channels in the tau2 transmission pattern equal to zero.

2.6 The match function in dual-frequency experiments

The standard EISCAT experiments tau1 and tau2 use two frequency channels. In the derivation of the MF method, we stated that the approach applies unmodified to *all* transmissions. But we also said that for numerical efficiency, we have to apply approximations to the signal model. Our approximation is good only for single-channel data. For the actual two-channel data the approximation breaks down, the more badly the larger the target velocity is, and the longer the integration time. The break-down causes the estimated signal amplitude to fall below the ideal, fully coherently integrated, value. With our standard 300 ms integration time, for targets with Doppler-velocities larger than about 2 km s^{-1}, we are only marginally more sensitive than if we were making use of only a single channel's data. For example, in Fig. 4 we show the integrated amplitude as a function of target velocity for 300 ms integration in the tau2 experiment. In the figure, we show the maximum value of the noiseless FMF (strongly oscillating dark curve) and the MF (the dark-coloured envelope curve, with wide line width) as a function of target radial velocity. Value of unity represents fully coherent integration. The light-coloured curve, with values little less than 0.5 independent of target velocity, is the integrated amplitude when one omits one of the two frequency channels from the coherent integration.

3 Measuring system

3.1 Hardware

The EISCAT UHF radar

So far in our SD measurements we have used the EISCAT UHF radar. The 32 m UHF antenna has a fully steerable parabolic dish, Cassegrain optics, and features rotation rate of about 80°/min both in azimuth and elevation. The antenna pointing direction is calibrated using celestial radio sources, and is believed to be accurate better than 0.1° in most directions.[5]

A block diagram of the UHF radar at the Tromsø site is shown in Fig. 5. The Tromsø UHF receiver has a cooled preamplifier, giving a system temperature $T_{\mathrm{sys}} \approx 110$ K. The radar's radio-frequency (RF) band is centered at 928 MHz, and there are 14 transmission frequencies available, 300 kHz apart. In the most common EISCAT experiment modes, two frequency channels are used. Recently those have been centered at 929.9 MHz (EISCAT frequency F13) and 930.2 MHz (F14). The RF signal is mixed in two stages to the second intermediate frequency (IF2) band, using local oscillators at 812.0 MHz and 128 MHz, so that F13 maps to 10.1 MHz and F14 to 9.8 MHz. The band is formed by the radar's antialiasing filter, which is 6.8 MHz wide and centered at 11.25 MHz.

In the standard EISCAT data processing, the second IF is digitized by a 14-bit analog-to-digital converter (A/D), which produces a continuous sample stream at the rate of 15 Msamples/s. The stream of IF2 samples is distributed to the multi-channel, VME-based, EISCAT digital receiver, each channel occupying one slot in a VME crate. Custom hardware in each channel performs quadrature detection, followed by sampling rate reduction appropriate to the typical 10–50 kHz final channel bandwidth. The baseband sample stream is buffered, and further processing to averaged sample-correlation products is done on UNIX-based computers.

The EISCAT UHF transmitter consists of a programmable radar controller that generates the pulse patterns at DC level, either uncoded on/off pulses or various classes of binary phase codes; an exciter system that converts the radar controller output to RF around 928 MHz; and a klystron power amplifier that consists of two klystron tubes, in principle capable of delivering a combined peak power of about 2.5 MW. The power during all our space debris measurements has been considerably lower, at 1 to 1.5 MW. The maximum transmitter duty cycle is 12.5%, and duty cycles near this value are also used in most experiments in practice. The time and frequency base at all EISCAT sites is taken from the GPS system.

The space debris receiver

To be able to use our own data processing, optimized for hard targets, we use a special digital receiver back-end, the space debris receiver. The signal to the space debris receiver is branched off from the EISCAT analog signal path at the second IF (IF2) level. Figure 5 shows the main blocks of the SD receiver, connected to the EISCAT UHF system at the Tromsø site.

[5] The UHF antenna has the half power beam width 0.6°. The official EISCAT pointing program uses geocentric cartesian coordinates $x = 2106.791$ km, $y = 734.793$ km, and $z = 5955.183$ km for the antenna, while assuming a reference spheroid with semimajor axis 6378.135 km and semiminor axis 6356.75 km. The corresponding geographic coordinates are latitude 69.586°N, longitude 19.227°E, and altitude 0.086 km.

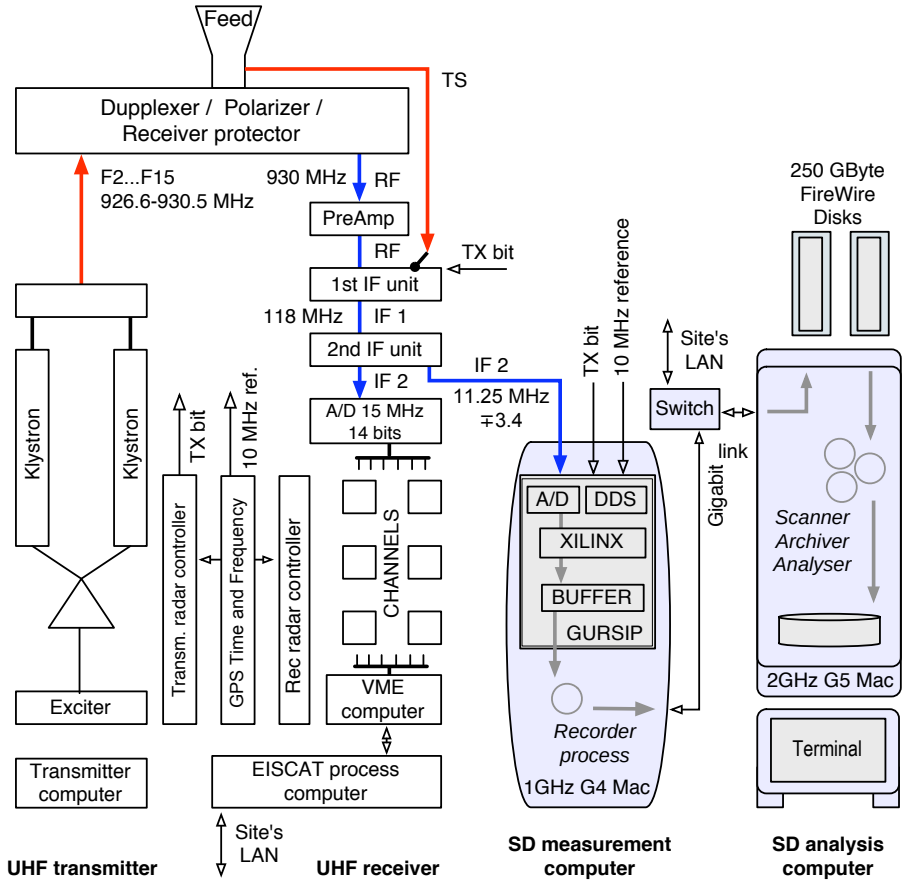

Figure 5: The space debris receiver connected to the EISCAT UHF radar. The SD receiver consists of a measurement computer and an analysis computer. The measurement computer hosts a custom signal processing board (GURSIP). The primary analog input to the SD receiver is the EISCAT second intermediate frequency (IF 2) band. The input contains, time-multiplexed, both the standard received signal and the transmission sample signal (TS). On the processing board, there is an analog-to-digital converter (A/D) taking 40 megasamples per second; a direct-digital-synthesizer chip (DDS), which provides clock signals on the board, phase-locked to the host radar's 10 MHz frequency reference signal; two Xilinks signal processing chips (XILINX) to perform signal demodulation and sampling rate reduction; and a memory buffer for temporary storage of the samples. The recorder program running on the measurement computer moves the samples over a gigibit network link to an external FireWire disk, mounted on the analysis computer. Target detection is done by the scanner program running on the analysis computer, using the FMF-algorithm. After detection, two other software modules, the archiver and the analyser, store away the event's raw data, and estimate and save the target parameters.

The EISCAT standard data processing handles a multi-frequency transmission by feeding the IF2 data to multiple hardware channels, each tuned to a particular center frequency. Our approach in the SD receiver is different. We sample the analog IF2 band fast enough to capture the relevant frequency channels into a single digital stream. This type of data is called multichannel complex data in [6]. According to the bandpass sampling theorem, we need to take B million complex samples per second, in the minimum, if the spread of frequencies is B MHz. For our most often used measuring mode, where there are two frequency channels 300 kHz apart, we have normally used 500 kHz sampling rate. But we have also verified that the SD receiver can handle sampling speeds up to 2.5 Msamples per second.

In addition to the standard reception, our data processing requires that the transmission waveform is measured. As indicated in Fig. 5, EISCAT provides the transmission sample signal (TS) time-multiplexed into the same data path as the reception. The multiplexer switch is controlled by the receiver protector bit ("TX bit"), generated by the EISCAT radar controller microprocessor. We routinely record the receiver protector bit into our data stream to mark out the transmission blocks. The bit is stored into the least significant bit of the imaginary part of the $16 + 16$-bit complex integer data words. With this arrangement, the transmission signal gets sampled with the same rate as the actual reception (though we would actually like to sample it with a higher rate).

The core of the data acquisition system is a custom PCI-board which performs sampling, quadrature detection and sampling rate reduction. The board was developed originally for ionospheric tomography by the now defunct Finnish company Invers Ltd.

The A/D converter on the PCI board samples at 40 MHz. The resulting real-valued sample stream is processed by programmable logic chips, from the Xilinks SpartanXL family, to perform quadrature detection, essentially by doing Hilbert transform. The result of the transform is a complex-valued sample stream at 10 MHz rate, representing the negative frequency part of the spectral contents of the analog input. The chip then decimates the 10 MHz stream to the final sampling rate. Typical decimation factor M is 20, which yields 500 kHz final sampling rate. The decimation is done by adding samples in blocks of M; this ensures proper filtering.

It may be noted that there is no separate multiplication to baseband in this scheme. Instead, the customary frequency component at baseband is created by the undersampling. With the 40 MHz primary sampling rate, the arrangement requires that the band-limited analog input is centered at 10 MHz. Although it is possible to run the A/D converter on the board at other sampling rates, the 40 MHz is a most convenient choice. That the two frequencies EISCAT nowadays most often use in the standard measurements, are 10.1 MHz and 9.8 MHz, is a lucky coincidence. The next version of the SD receiver should have a complex mixer built-in.

The PCI board is mounted in a Macintosh G4 workstation, running under the Mac OS X version of UNIX. We call the Mac G4 the measurement computer. In addition, there is a dual-CPU Mac G5 computer for data analysis. The Mac workstations are connected to each other via a gigabit Ethernet link, and are also connected to the site LAN. The measurement computer runs software from Invers Ltd to read the sample data from an onboard buffer and write them to a hard disk, either a local disk, or a disk mounted over the gigabit link from the analysis computer. The data accumulation rate to the disk is between 7 and 30 GBytes per hour (2 to 8 MBytes s^{-1}), depending on the sampling rate. The maximum sustainable transfer rate over the data link in this configuration is more than 20 MBytes s^{-1}, so even 8 MBytes s^{-1} is only a minor load, and does not

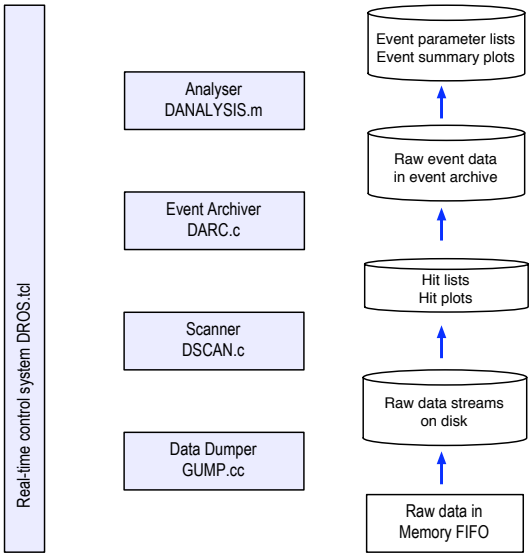

Figure 6: Main modules of the real-time SD data processing software.

affect significantly the computing performance of either of the workstations. The LAN connection is used to access the EISCAT process computer, to update the time base in the G4 and G5 once every 5 minutes, using the standard network time protocol (ntp). This ensures that the time base in the Macs stays within 20 ms of the time kept in the EISCAT system. This is more than adequate for time-stamping space debris events.

3.2 Software

An overview of the real-time SD data processing software system is shown in Fig. 6. The system consists of four main processing units and an overall control system. The processing has the following phases.

Sampling and demodulation. The SD receiver's programmable firmware delivers complex-valued baseband samples at a strictly regular rate to a buffer, which is visible in the measurement computer's memory space. The buffer is large enough to smooth out the less predictable access times of the reading process—which is an ordinary time-sharing UNIX process—so that no samples are lost.

Recording. The recorder program GUMP, provided by Invers, reads the data from the buffer and dumps them to disk files. The sample data are organized into directories which we call the stream directories, or just the streams. Typically, a stream contains 60 minutes of uninterrupted sample flow in time-stamped files, each storing one million complex points as $2 + 2$ byte integers.

Scanning. The streams are processed, one stream at a time, by the SD scanner program DSCAN. Two scanners can be running in parallel in the dual-processor analysis computer. The scanner reads a segment of raw data from a stream and searches through the segment for hard targets, range gate by range gate, performing threshold detection using the FMF algorithm. When a pre-determined threshold is exceeded, we say that we have a hit. The scanner saves the hit's description to a

file and proceeds to the next data segment. Scanning is the most time-consuming step in the data processing. Therefore, DSCAN is implemented as a C program that makes use of the AltiVec vector processor onboard the G5, by calling routines in Apple's DSP library (vdsp). The scanner performance depends strongly on the length of the input data vector. For the most common configuration (2 μs sampling interval and 0.3 s coherent integration), we get about 2 GFlops mean speed per processor (see Table 1).

Event archiving. The next module in the processing chain, the event archiver DARC, inspects the stream's list of hits, and combines to an event the hits that correspond to a single target passing through the radar beam. Having determined the time boundaries of the event, the archiver copies the event's data to a separate event directory. The event archiver is a C program, but it is not performance critical. Most of its time goes to data copying, so its speed is mainly limited by disk speed. We have saved all raw data from most of the test measurements so far—somewhat less than a terabyte—but in routine measurements, at most the raw data of events will be saved. With the event rates observed in the test measurements, saving all events from the more than 400 hours of measurements that we anticipate to be able to do annually, would require (only) on the order of a terabyte of storage per year.

Parameter estimation. As the last step, the analyser program DANALYSER picks events from the event directories and deduces and saves the event parameters. The method to compute the target parameters is still under development. What the analyser does now, is basically to call DSCAN to re-scan the data using FMF, but with maximum time and range resolution, over a narrow range interval, and to make linear or quadratic fits to the range and Doppler-velocity time series. The range and velocity parameters that we normally quote are taken from these fits, for the time instant of maximum signal strength. The analyser is a Matlab program.

The combined processing speed is such that for data taken with 2 MHz sampling rate, with 0.3 s coherent integration it takes 40–45 minutes to scan, archive and analyse one hour of raw data, while simultaneously accumulating new data. We need to make use of both CPU's in the analysis computer in this case. For the more typical 500 kHz sampling rate, we need only about 20 minutes to handle an hour, and then we need to use only a single DSCAN. The software system's performance under the benchmark load is summarized in Fig. 7.

An example of DSCAN performance during real operation is shown in Table 1. The table shows the performance info printed out by DSAN after it has processed a stream. The measurement was done during a test campaign in March 2004. The EISCAT experiment was tau1 and the SD receiver was sampling with 2000 ns sampling interval. The two scanners had no problem in keeping up with real-time. Each scanner processed 0.3 seconds of data and then skipped 0.2 seconds; a period of 192 ms was required to handle one second of input data. Clearly, even a single scanner would have been enough for real-time speed, and there is no need for any skipping of data either.

Internal timing of the FMF evaluation subroutine FASTGMF, invoked from DSCAN, is shown in Table 2. The lines 18 to 21 of the table give the time spent per range gate in the main steps of the FMF (Fig. 3). The test was done on a 1 GHz G4 Mac; a 2 GHz G5 Mac is almost twice as fast. Table 2 shows that for short, cache-friendly data vectors,

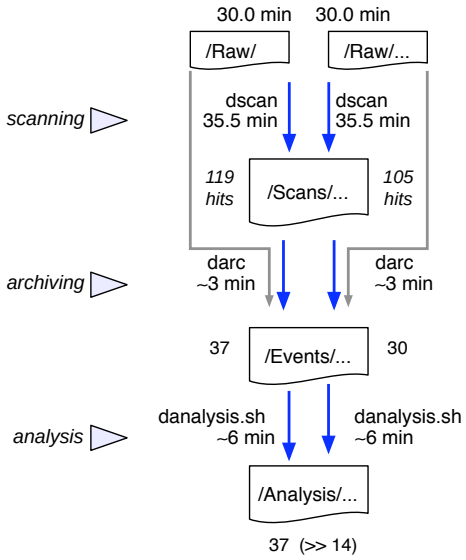

Figure 7: Software performance under benchmark load. The figure shows the time required by the scanner, archiver, and analyzer, running on the G5 analysis computer, to handle 60 minutes of data, composed of two 30 minute data sets on a disk. During the test, new data was being transferred with the benchmark rate of 27 GBytes h^{-1} from the measurement computer to the analysis computer. The two sets were processes in parallel by the two processors of the G5 workstation, and both required about $35.5 + 3 + 6 = 45$ minutes to complete.

Table 1: DSCAN speed when scanning tau1 2 μs data with the FMF. Both the recorder GUMP and two DSCAN scanners were active simultaneously. The recorder wrote samples at the rate of 2×10^6 Bytes s^{-1} over the network to the same FireWire disk on the analysis computer from which the two scanners read it. The combined processing speed was about 4000 MFlops.

```
scanner 1
  7318 scans -- 1400.0 sec -- 98 hits
  Time per scan : 191 ms
  Read per scan : 41.6 ms 0.60 MBytes 14.3 MBytes/s
  Time per gate : 0.260 ms
  FMF per gate  : 0.199 ms 0.398 MOp 2000 MFlops
scanner 2
  7318 scans -- 1405.2 sec -- 135 hits
  Time per scan : 192 ms
  Read per scan : 41.5 ms 0.60 MBytes 14.3 MBytes/s
  Time per gate : 0.261 ms
  FMF per gate  : 0.200 ms 0.398 MOp 1993 MFlops
```

Table 2: Performance of DSCAN when scanning tau2 data (taken with 2 μs sampling interval) using the FMF, with 312 ms coherent integration. This test was done on a 1 GHz G4 Mac. The FFT speed is 5600 MFlops, delivered by the AltiVec-boosted library routine on 4 kword input vector. The complex multiplication proceeds only with the speed of 550 MFlops. In spite of the fast FFT, the overall FMF processing speed is only 1050 MFlops. To handle 686 range gates, giving range coverage 345–1575 km (a gap excluded), took 323 ms, which is a trifle longer than the 312 ms long input data segment.

```
1  Scan parameters
2    sampling    2000 ns
3    integration 156240 (312.480 ms)
4    n to read   158988
5    n ipps      56 (28 cycl)
6    n per tx    288
7    n shifts    686
8  FMF parameters
9    n fftin     4032
10   fft length  4096 (2^12)
11 Scanner timing
12   Time/scan  323 ms
13   Time/gate  0.470 ms
14   FMF/gate   0.403 ms 0.424 MOp 1053 MFlops
15 FMF internal timing per range gate
16   Operation              N      Op      us    MFlops
17   ------------------------------------------------
18   x(t)*y(t)          56*288   96768     176       550
19   Sum xy_n           56*288   32256     127       250
20   X(t)*e^(iat_0^2)    56*72   24416(a)   74       330
21   FFT                  4096  270486      48      5600
22   Total                      423926     425(b)   1000
23   --
24   a) 56*4 + 4032*6
25   b) Measured FMF/gate was 488 us.
```

the library FFT, which uses the vector processor, is quite fast: the 4096 point FFT that we normally use gives about 5000 MFlops per processor. In fact, most of the FMF processing time is spent elsewhere than in the FFT. For the long data vectors used in the MF, processing speed is limited by the (now much slower) FFT speed. For instance, a 2^{20} point FFT proceeds with only 410 MFlops. We use the vectorized library also for complex multiplication (line 18 in the table), but there the speed is disappointingly low.

The four main processing blocks run as independent, stand-alone UNIX timesharing processes, which do their specific job once and then die. The processes themselves do not know anything about each other. The processing chain is created and organized by software that we call DROS. The name is a modified version of EROS, and is meant to indicate that the DROS system is a slightly tailored copy of the standard EISCAT real-time radar operating system of that name. Based on an experiment-specific configuration file and a given start time, the DROS system generates the required input files and command line parameters for the processing modules, starts and restarts the processes in the two computers as required, and maintains and logs state information. The DROS system can query the running EROS at the host radar to find the antenna pointing direction and transmission power information.

4 Measurements

In this section we show examples of the results of the measuring campaigns. To incorporate recent updates in the analysis procedure, we re-analysed all the data sets, both using the FMF and the MF algorithm. We did not re-scan the raw data, but the starting point was the set of events found in the original detection scans. A consequence is that the range coverage of the data vary, for we realised only late that it is useful to monitor higher than LEO regions even when the primary interest is in LEO.

In the measurement campaigns, all conducted at the EISCAT UHF radar in Tromsø, two EISCAT experiment were used, the tau1 and tau2 experiments. We conducted two test measurement campaigns as stipulated in our work contract, the first in October 2003, the second in March 2004. In addition, we took part to the beam park 2004 multi-radar SD measurement campaign, by a 16 hour run in September 2004. Finally, we measured four days during a standard EISCAT CP1 experiment in November 2004. The data sets are the following.

1. *oct03-tau1-2000*: 10.6 hours, 232 events, of tau1 data, recorded in three intervals in October 13, 14 and 16, 2003, using 2000 ns sampling interval in the SD receiver.

2. *mar04-tau1-2000*: 13.9 hours, 286 events, of tau1 data, recorded between 11:30 UT, March 4 and 01:00 UT, March 5, 2004, using 2000 ns sampling interval.

3. *mar04-tau2-2000*: 10.9 hours, 146 events, of tau2 data, recorded 01:00–11:00 UT, March 5, and 14:50-16:00 UT, March 10, 2004, using 2000 ns sampling interval.

4. *mar04-tau2-500*: 5.4 hours, 102 events, of tau2 data, recorded 08:30–14:00, March 10, 2004, using 500 ns sampling interval.

5. *sep04-tau1-2000*: 16.6 hours , 368 events, of tau1 data, recorded from 15:49 UT, September 7, to 08:29 UT, September 8, 2004, using 2000 ns sampling interval.

6. *nov04-tau2-2000*: 100 hours, 1518 events, of tau2 data, recorded from 09:02 UT, November 09, to 14:00 UT, November 13, 2004 using 2000 ns sampling interval, during a standard EISCAT ionospheric experiment.

For the *sep04-tau1-2000* data, the Tromsø UHF antenna was pointed to azimuth 133.3°, elevation 61.6°; for all other data sets, the antenna was pointed along the magnetic field direction, azimuth 184.0°, elevation 77.1°.

Figure 8 shows the target detection rate as a function of altitude for two data sets, in 50 km bins. We indicate by cross-hatching the altitude regions where targets were not looked for. Bins adjacent to those regions have artificially low detection rates. In the tau1 data set, the well-known generic features of the LEO SD data are reproduced, with a maximum around 900 km altitude and another maximum developing, but not fully visible, towards 1500 km altitude. The tau2 data set has a maximum at 1000 km, but there is a data gap at precisely those bins where the tau1 data have their maximum. Nevertheless, the peak event rate is about 2.5 events/hour/bin in both cases.

Figure 9 shows the effective diameter as function of altitude and gives the relative frequency of the diameters. The detection sensitivity is about 2 cm at the 1000 km range. As a curiosity, we note a small discontinuity in all the panels of Fig. 9 at about 6 cm diameter. This feature is most probably an artifact due to our definition of the effective diameter. Our definition ignores the resonance region in the scattering and

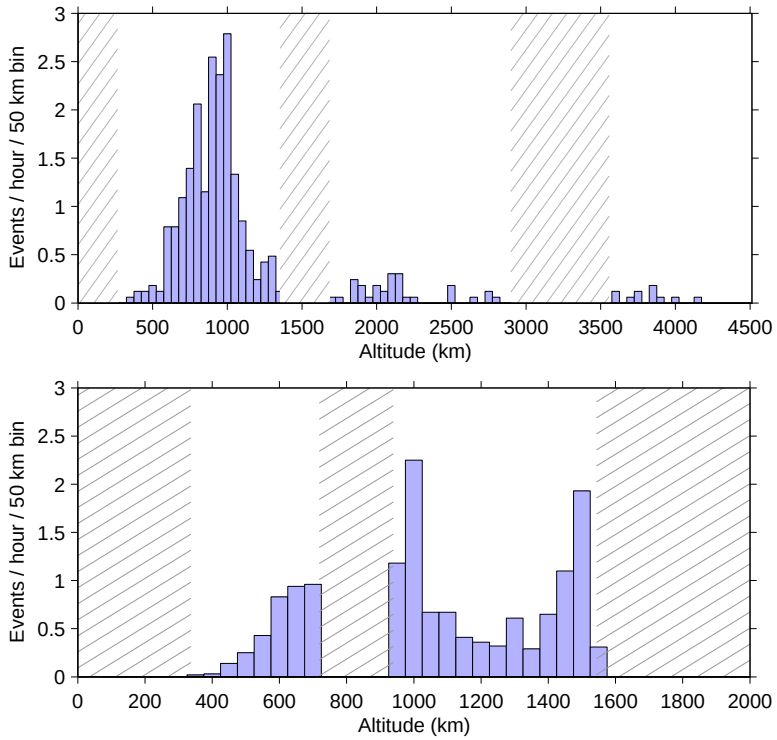

Figure 8: Event rate versus altitude. The data sets are *sep04-tau1-2000* (368 events) and *nov04-tau2-2000* (1518 events).

accordingly, we change the formula that converts from the radar cross section to the effective diameter, abruptly at 5.9 cm.

Figure 10 shows the Doppler-velocity v_{D} in the *nov04-tau2-2000* data set, analysed both with the FMF (top panel) and the 100 times slower MF (the middle panel). Not much can be gained by using the MF in the analysis. In the bottom panel we show the radial velocity v_{RR}, fitted from the $R(t)$ time series data. The v_{RR} data is intented for sanity check only; the v_{D} data should normally be used for the radial velocity. The analyser does not attempt to determine v_{RR} if there are too few good points $R(t_n)$ available. The v_{RR} is nominally computed in 85–90% of the events, but many fits are quite bad, and it is not surprising that the v_{RR} data show more scatter and less structure than the v_{D} data. For instance, the splitting of the "towards" ($v_r < 0$) and "away" data into two closely separated stripes, very visible in the v_{D} data in the middle panel of Fig. 10, is barely observable in the corresponding v_{RR} data in the bottom panel of Fig. 10.

Figure 11 shows radial acceleration, computed by linear fit to the velocity time series $v_{\mathrm{D}}(t)$, when enough data points are available. As we have indicated in the figure, this happened only in about two thirds of the events. We have also plotted the acceleration value that was used in the detection scans. The acceleration value is represented by the upper edge of the shaded arc and corresponds to circular-orbit and strictly vertical pointing. The lower edge of the arc is computed assuming that the antenna is pointed towards south, at the elevation that was actually used, and that the target is moving in circular polar orbit across the beam. The shaded region should therefore be representative of the possible values of radial acceleration of targets in circular orbits. However,

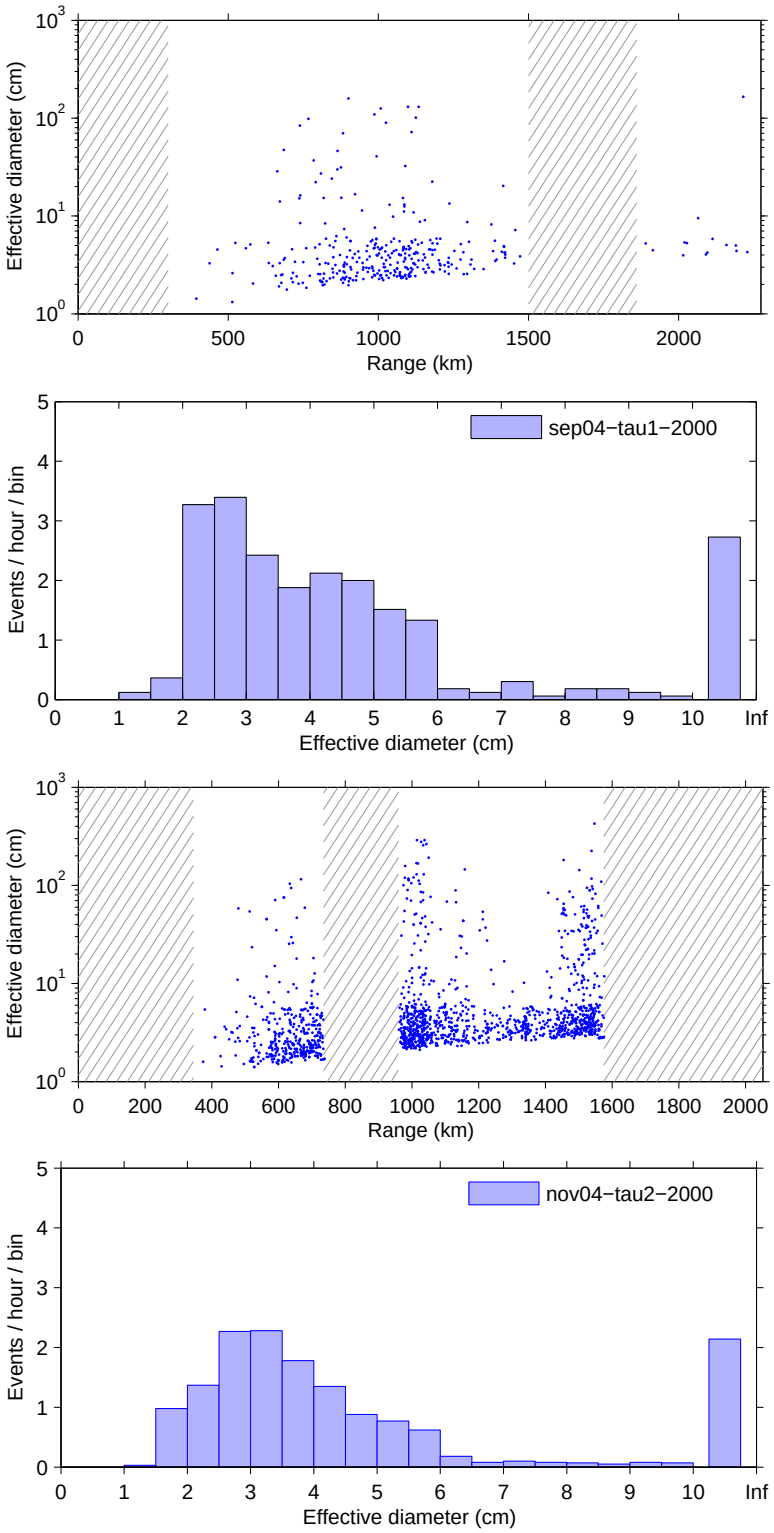

Figure 9: Effective diameter. The data sets are *sep04-tau1-2000* (top two panels) and *nov-tau2-2000* (bottom two panels).

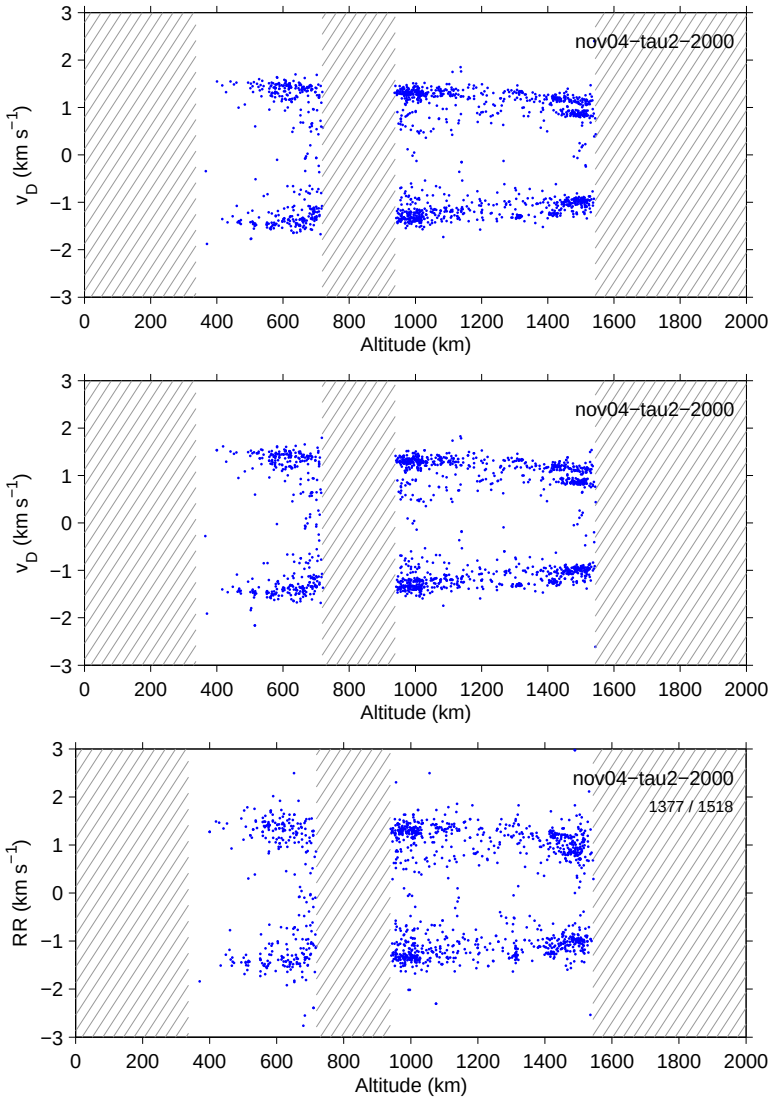

Figure 10: Radial velocity in *nov04-tau2-2000* data, analysed in various ways. The plotted value is v_{D} in the top two panels, and v_{RR} in the bottom panel. The top panel data are analysed using FMF, the other two panels are analysed using MF.

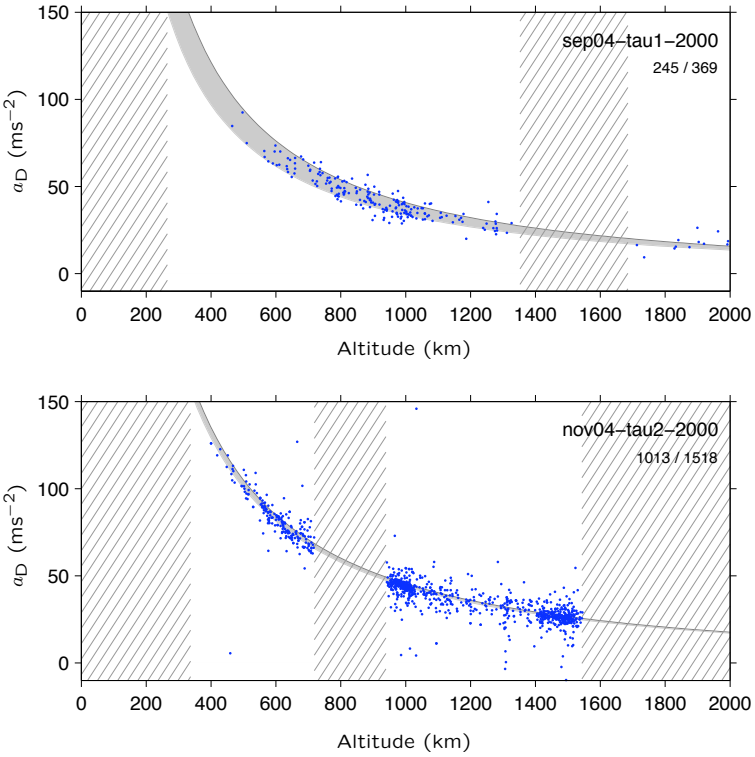

Figure 11: Radial acceleration a_D.

much of the scatter in the data points is more likely due to bad fits than the targets actually being in non-circular orbits.

Acknowledgements

In the late Lappish Summer 2004, our colleague and friend Juha Pirttilä died. In 2000, Juha wrote the initial MEX implementation of the MF algorithm, which showed that the present work might become possible. The development of his GUMP program that launches every time we do a measurement with the SD receiver is frozen now; there is no need to modify the program; in the shape he left it, it will be supporting this work a long time into the future. Juha was one of the kindest persons we have ever worked with; his entirely untimely demise is a loss that we are finding hard to cope with.

The EISCAT facility is supported by Finland (SA), France (CNRS), the Federal Republic of Germany (MPG), Japan (NIPR), Norway (NFR), Sweden (NFR), and the United Kingdom (PPARC).

References

[1] M. Baron, The EISCAT facility, *J. atmos. terr. Phys.* **46** (1984) 469.

[2] M. Baron, EISCAT progress 1983–1985, *J. atmos. terr. Phys.* **48** (1986) 767.

[3] ESA Directorate of Technical and Operational Support ESOC Ground Segment Engineering Department Mission Analysis Section, *Study specification, measurements of small-size debris with backscatter of radio waves* (Darmstadt, Germany, 1999).

[4] ESA Directorate of Technical and Operational Support ESOC Ground Segment Engineering Department Mission Analysis Section, *Study specification, real-time space debris detection with EISCAT radar facilities* (Darmstadt, Germany, 2002).

[5] M. Lehtinen, Statistical theory of incoherent scatter radar measurements, *EISCAT Techn. Note* **86/45** (Eur. Incoherent Scatter Sci. Assoc., Kiruna, Sweden, 1986).

[6] M. Lehtinen, J. Markkanen, A. Väänänen, A. Huuskonen, B. Damtie, T. Nygren and J. Rahkola, A new incoherent scatter technique in the EISCAT Svalbard radar, *Radio Sci.* **37** (2002) 3-1.

[7] B. R. Mahafza, *Radar system analysis and design using MATLAB* (ChapmanHall/CRC, 2000).

[8] J. Markkanen, M. Lehtinen, A. Huuskonen and A. Väänänen, Measurements of Small-Size Debris with Backscatter of Radio Waves, (Final Report, ESOC Contract No. 13945/99/D/CD, March 2002).

[9] M. I. Skolnik, *Introduction to radar systems* (second edition, McGraw-Hill, Singapore, 1981).

[10] G. Wannberg, I. Wolf, L.-G. Vanhainen, K. Koskenniemi, J. Röttger, M. Postila, J. Markkanen, R. Jacobsen, A. Stenberg, R. Larssen, S. Eliassen, S. Heck and A. Huuskonen, The EISCAT Svalbard radar: A case study in modern incoherent scatter radar system design, *Radio sci.* **32** (1997) 2283.